Quantitative Atomic-Scale Analysis of Interface Structures: Transmission Electron Microscopy and Local Density Functional Theory

S. Nufer, A. G. Marinopoulos, T. Gemming, C. Elsässer, W. Kurtz, S. Köstlmeier, and M. Rühle
Max-Planck-Institut für Metallforschung, Seestraße 92, D-70174 Stuttgart, Germany
(Received 6 September 2000)

Transmission electron microscopy (TEM) and local density functional theory (LDFT) are combined to analyze the microscopic structure of the rhombohedral twin interface in α-Al_2O_3. LDFT provides interfacial energetics and atomic and electronic structures for three competing models. With high-resolution TEM the atomic structure at the interface is imaged quantitatively along two orthogonal zone axes. Electron energy loss spectroscopy in TEM with nanoscale spatial resolution yields the interfacial electronic structure. Both experiments confirm the theoretically preferred model quantitatively.

DOI: 10.1103/PhysRevLett.86.5066 PACS numbers: 61.72.Bb, 61.72.Ff, 71.15.–m, 73.20.–r

I. Introduction.—Transmission electron microscopy (TEM) is one of the most powerful experimental approaches to study extended structural defects such as dislocations or grain boundaries buried in the interior of real materials [1,2]. Various structural and functional properties of technologically important materials, with polycrystalline or layered microstructures, are controlled or influenced by the atomistics, bonding, and energetics at the internal boundaries. Therefore, it is of high importance to characterize and understand the atomistic and electronic structure at an atomic scale not only of single-crystalline compounds but of interfaces as well.

Interfacial *electronic structures* can be explored with scanning transmission electron microscopy by electron energy loss spectroscopy (STEM-EELS) with high resolution, of both about 1 nm spatially and 0.5 eV energetically [2]. The energy-loss near-edge structures (ELNES) in EELS provide characteristic features about the local elemental composition, electronic states, bonding, and coordination. Alternatively, first-principles electronic-structure and total-energy calculations based on the local density functional theory (LDFT) [3,4] provide very accurate and predictive theoretical information about structures and properties of bulk crystals, surfaces, and interfaces [5,6]. Local electronic structures for comparison with ELNES are derived from the one-electron eigenvalues and wave functions via site and angular-momentum projected densities of states (PDOS), which are related to the double differential cross section for inelastic electron scattering [7,8]. Theoretically predicted *atomistic structures* are quantitatively compared to high-resolution transmission electron microscopy (HRTEM) images via image simulation [9,10].

In the present study, first-principles LDFT calculations, employing a mixed-basis pseudopotential approach [11–13], and STEM-EELS experiments are employed to investigate the atomic arrangement and electronic structure at an interface in α-Al_2O_3 (sapphire, corundum). Quantitative HRTEM is used to verify the atomic arrangement. The considered interface is the rhombohedral twin boundary. It is aligned parallel to a $(\bar{1}012)$ plane of the corundum structure. The rhombohedral twin, alternatively to the basal twin, is of major interest for plastic twinning deformation of α-Al_2O_3 crystals.

In a recent LDFT study of the rhombohedral twin interface [14] three metastable configurations were found which represent local energy minima with respect to axial and lateral translations of the two grains. The twin configuration with the lowest interface energy, $E_{\text{int}} = 0.63\ \text{J/m}^2$, is terminated by the "vacant" octahedral interstitial cation positions in the oxygen sublattice, i.e., those not occupied by Al cations (cf. Ref. [14]). The two grains are mutually related by screw-rotation symmetry. Thus, this structure is denoted as S(V) (screw-rotation symmetry with "vacancy" termination). Another twin structure with vacancy termination and glide-mirror symmetry, G(V), has a high interface energy $E_{\text{int}} = 3.34\ \text{J/m}^2$. The third twin interface, G(O), is terminated by an oxygen layer, shows again glide-mirror symmetry, and has an interface energy of $E_{\text{int}} = 1.35\ \text{J/m}^2$. Therefore, the structure S(V) and its electronic states are predicted to be most favorable by LDFT. The structural details of the three interface models are displayed in Figs. 1, 4 and 6 of Ref. [14]. The unrelaxed interface model proposed earlier in Fig. 2 of Ref. [15] corresponds to the high-energy model G(V) (cf. Fig. 4(b) of Ref. [14]).

This case study of the rhombohedral twin demonstrates the progress achieved in the field of experimental ELNES. Only recently LDFT based calculations of ELNES for ceramic materials have reached a level of accuracy sufficient for interpretation of measured bulk spectra [8,16]. Meanwhile, experimental ELNES investigations have matured to a degree that allows one to distinguish and decide between different structure models of a grain boundary, the results being consistent with results of LDFT based structure calculations and with HRTEM results.

 0031-9007/01/86(22)/5066(4)$15.00

II. Electron energy loss spectroscopy in a STEM.—For STEM-EELS and HRTEM studies, a rhombohedral twin bicrystal was made by diffusion bonding [17] of two suitably oriented crystals of highly pure sapphire in ultra-high vacuum. No contamination at the interface was detectable by energy-dispersive x-ray spectroscopy in the STEM. Electron and x-ray diffraction measurements indicated deviations of $\sim 0.1°$ off the perfect orientation relation. The TEM specimens were prepared using diamond wire saw, grinding polisher, dimple grinder, and ion milling. The specimens used to determine the results presented here were ion milled at only 2.5 keV in order to minimize their susceptibility to irradiation damage in the TEM. More conventional milling at higher energies resulted in specimens for which the eventual radiation damage inhibits a meaningful comparison between experimental and theoretical grain-boundary ELNES.

The EELS experiments were performed with a dedicated STEM (VG HB501UX), run at 100 kV and equipped with a parallel EELS spectrometer. Bulk and interfacial EELS were acquired in a spot modus, with an energy dispersion of 0.1 eV per channel and an effective electron beam diameter of about 1.7 nm passing through the specimen. (The nominal spot diameter of the beam entering the specimen is 1.0 nm.) For every measurement, spectra were recorded at the interface region and in more remote bulk areas on both sides of the interface. Neither the spectra nor the subsequently recorded dark-field images indicated any evidence for specimen damages by electron irradiation. From the low-loss spectra local specimen thicknesses of 20 to 40 nm were determined.

All experimental sets of O K-ELNES showed the same features as the set of bulk and interfacial spectra displayed in Fig. 1. The interfacial spectra have lower intensities at the prominent peaks (marked by arrows) and rise already about 0.2 eV below the bulk edge onset. Applying the spatial difference method for interfaces [18], 85% of the bulk spectra were subtracted from the interfacial spectra, accounting for the number fraction of bulklike oxygen atom columns in the electron spot region. This resulted in interfacial ELNES like curve (b) in Fig. 1. This interface-specific part of the spectrum shows a splitting of the first peak around 540 eV and a broad feature between 550 and 560 eV energy loss. The shape of the difference spectrum does not change significantly for bulk subtractions within a range from about 80% to 90%. Also it is not merely an artifact of a subtraction of energy-drifted bulk spectra. Furthermore, LDFT results for all three interface models indicated that only the O-PDOS from sites directly at the interface differ strongly from the bulk O-PDOS. Thus, by a count of the O columns within a circular beam region of 1.7 nm diameter, with the interface crossing the center of the circle, a ratio of 83% bulk and 17% interface O columns for all three models is estimated. This ratio lies well within the given range of significance for the experimental spatial difference spectra.

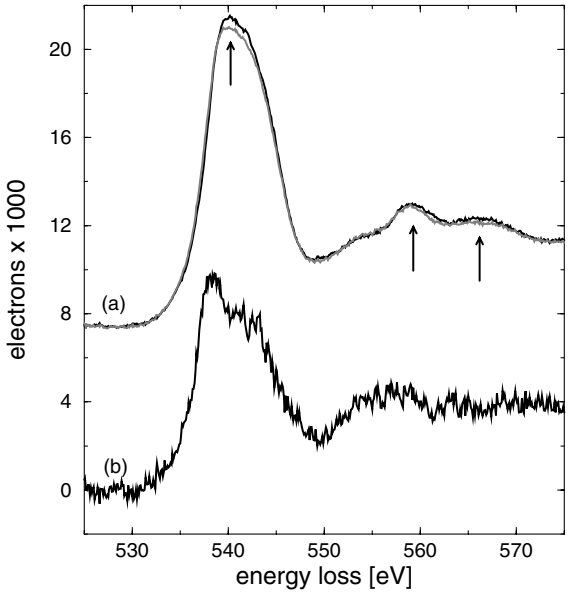

FIG. 1. Experimental oxygen K-edge energy-loss near-edge spectra of α-Al_2O_3: (a) bulk (black line) and interface (grey line) spectrum as measured (no background subtracted); (b) spatial difference spectrum obtained by subtracting 85% of the bulk spectrum from the interface spectrum of (a) (background subtracted). The prominent peaks are marked by arrows.

Assuming the dipole approximation for the inelastic scattering of electrons, in a one-electron approach like the LDFT the O p-PDOS of the unoccupied bands are related directly to the ELNES at the O K-edge [8]. Final-state effects of the $1s$ core holes formed by the excitation of core electrons to the conduction bands are incorporated by the $Z + 1$ approximation, where the excited oxygen atom O^* is mimicked by a fluorine atom [16].

Figure 2 displays the comparison of calculated p-PDOS of an excited O^* atom in bulk sapphire with an O K-edge ELNES obtained by EELS. In this and the following calculated p-PDOS a Gaussian broadening of 1.6 eV is applied, which gives the best visual agreement between calculated and measured spectra for bulk sapphire. The PDOS including final-state effects and the ELNES agree with respect to the number and energy positions of characteristic features [8] and also in their spectral strength [16]. Finer structures are hidden in this calculated p-PDOS. Their presence is illustrated in Fig. 2 by the other p-PDOS with a broadening of only 0.8 eV.

For a consistent determination of the interfacial structure from ELNES and LDFT, O^* p-PDOS were calculated for oxygen positions at the interface planes in the three metastable interface models of Ref. [14], in the same way as for the bulk O^* p-PDOS displayed in Fig. 2. In Fig. 3 the LDFT results are compared with the experimental interfacial O K-edge spectrum (cf. Fig. 1). Three independently acquired spatial difference spectra were added, and the sum spectrum was smoothed with a low-pass filter of 1 eV. A comparison of PDOS with ELNES excludes the

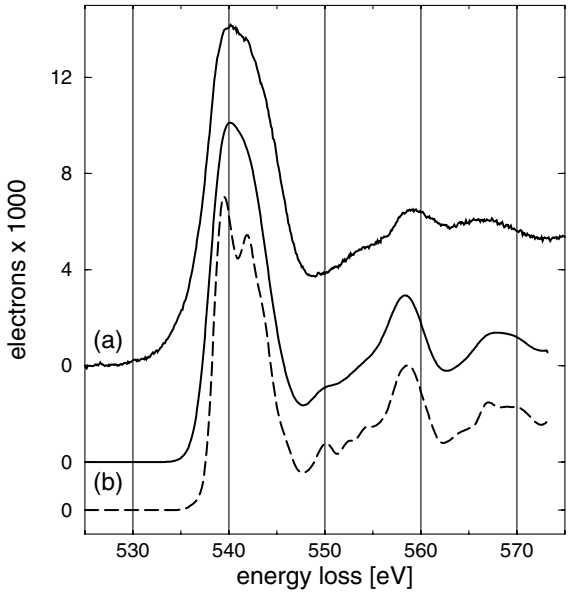

FIG. 2. Oxygen K-edge energy-loss near-edge spectrum of bulk α-Al_2O_3: (a) experimental spectrum; (b) calculated O^* p-PDOS of unoccupied conduction-band electron states with Gaussian broadening of 1.6 eV (solid line) and 0.8 eV (dashed line).

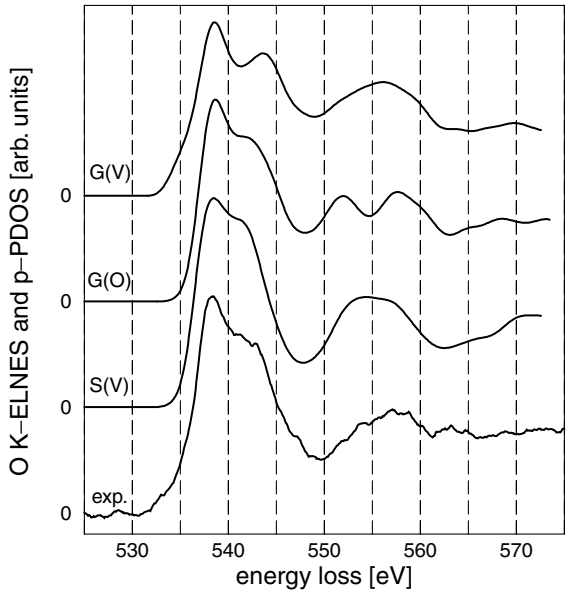

FIG. 3. Comparison of the experimental oxygen K-edge energy-loss near-edge spatial-difference spectrum at the interface (bottom curve, obtained by averaging three sets of spectra, cf. Fig. 1, and applying a low-pass filter of 1 eV for noise reduction) with calculated O^* p-PDOS of unoccupied conduction-band electron states at the oxygen sites closest to the interfaces (with Gaussian broadening of 1.6 eV) for the three models S(V), G(O), and G(V). The calculated curves are shifted in energy to match the first peak of the measured spectrum at 538 eV.

interface model G(V) because its PDOS displays too large a splitting of the two peaks around 540 eV. The interface model G(O) should be ruled out because the broad feature around 555 eV is split into two peaks in the calculated PDOS, but not in the experimental ELNES. Only the O^* p-PDOS of model S(V) agrees with the experimental O K-edge spectrum in the energy range up to 30 eV above the edge onset. Hence, with EELS it is possible to assess experimentally the structure and electronic states predicted by LDFT.

III. Quantitative high-resolution TEM.— HRTEM images of the bicrystal were recorded with the microscopes JEM 4000EX and JEM ARM-1250 [19], operated at 400 kV and 1250 kV, respectively, and with point resolutions of 0.17 nm and 0.12 nm, respectively. The same TEM specimens as for the EELS measurements were used. To differentiate between the three structure models HRTEM observations have been made along $[\bar{1}2\bar{1}0]$ and $[10\bar{1}1]$, which are orthogonal axes in the interface plane.

Figure 4 displays a section of an HRTEM image of the boundary projected along $[10\bar{1}1]$. The position of the interface is marked by the vertical line. It illustrates the very high quality of the diffusion-bonded bicrystal by displaying exactly the same image contrast patterns on both sides of the boundary. The interface can hardly be recognized in Fig. 4. Its location can be seen well by a small difference in brightness on the original image. The translational periodicity of the pattern does not change across the interface. According to the LDFT prediction this is consistent with only the models S(V) and G(O) and rules out the high-energy interface model G(V), for which a pattern with a mirror symmetry plane at the interface should appear (cf. Fig. 6(b) in Ref. [14]).

The HRTEM image of the bicrystal along $[\bar{1}2\bar{1}0]$ allows one to discriminate between the other two interface models. The quantitative analysis of this HRTEM image, displayed as panel (A) in Fig. 5, involves a matching with simulated images [20]. For optimum agreement, the imaging parameters (e.g., defocus, specimen thickness, lens aberrations, and transfer function of the recording medium)

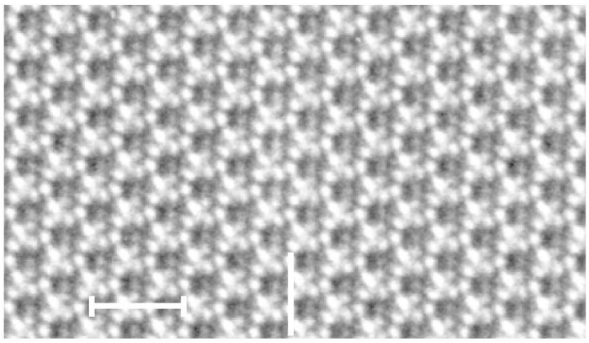

FIG. 4. High resolution transmission electron microscope image of the rhombohedral twin grain boundary along the $[10\bar{1}1]$ zone axis. The position of the interface plane $(\bar{1}012)$ is indicated by the vertical line. There is no apparent change in the image pattern across the interface. The length of the scale bar is 1 nm.

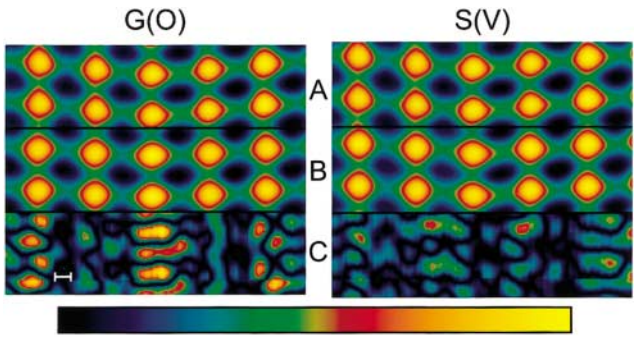

FIG. 5 (color). High resolution transmission electron microscopy images of the rhombohedral twin grain boundary along the $[\bar{1}2\bar{1}0]$ zone axis. The interface is located vertically in the middle of each image. (A) The experimental image (same left and right); (B) the best matching simulated image for the structure models G(O) (left) and S(V) (right); (C) the difference image, enhanced by a factor of 6, between experiment and corresponding simulation. The color scale marking relative image intensities from 0 to 1 (from left to right) is shown at the bottom. The length of the white scale bar in the left panel (C) is 0.1 nm.

were determined by variation [9,10]. Three separate optimizations were performed, employing the three theoretical interface models to initialize the image-parameter refinement. A measure of the success of a quantitative image matching is the cross correlation factor (XCF) in the pixel-by-pixel comparison of experimental and simulated images (XCF = 1 means both images are identical). The optimizations yielded XCF = 0.987 for the model S(V), 0.981 for G(V), and 0.973 for G(O). Since the structure G(V) was ruled out by inspection in Fig. 4, the better match indicates that model S(V) is the most likely one. This can also be seen in panel (C) of Fig. 5 where the difference between experimental [panel (A)] and simulated [panel (B)] HRTEM image for G(O) is considerably larger than for S(V) at the interface. Additionally, the image parameters determined by variation for G(O) are not consistent with the known and fixed instrumental conditions of the TEM during the image recording. Thus, quantitative HRTEM determines the structure S(V) for the bicrystal. This independent result is in complete agreement with the previous conclusions of LDFT and of STEM-EELS; i.e., the structural model S(V) is the most appropriate one for the rhombohedral twin interface.

IV. Conclusion.—This study evaluates the feasibility to predict and to measure the electronics of an interface structure at an atomic level. By comparison of calculated projected densities of electronic states and measured ELNES a consistent and unequivocal decision about the microscopic interfacial structure is achieved that is verified by quantitative HRTEM. This is demonstrated here for the case of the rhombohedral twin interface in sapphire.

Of three proposed structure models, S(V) is the preferred interface structure owing to its theoretically lowest interface energy, to its agreement of the experimental O K-edge ELNES with the theoretical O^* p-PDOS at the interface, and to the quantitative HRTEM image matching along two orthogonal zone axes parallel to the interface plane. These results illustrate that LDFT and ELNES can determine quantitatively the electronic structure as well as the geometric translation state and local atomistics of interfaces with high precision.

This work is supported by the Deutsche Forschungsgemeinschaft (Project No. El 155/4-1).

[1] F. Ernst, Mater. Sci. Eng. **R14**, 97 (1995).
[2] D. A. Muller and M. J. Mills, Mater. Sci. Eng. **A260**, 12 (1999).
[3] P. Hohenberg and W. Kohn, Phys. Rev. **136**, B864 (1964).
[4] W. Kohn and L. J. Sham, Phys. Rev. **140**, A1133 (1965).
[5] R. O. Jones and O. Gunnarsson, Rev. Mod. Phys. **61**, 689 (1989).
[6] W. E. Pickett, Comput. Phys. Rep. **9**, 115 (1989).
[7] M. Nelhiebel, P.-H. Louf, P. Schattschneider, P. Blaha, K. Schwarz, and B. Jouffrey, Phys. Rev. B **59**, 12 807 (1999).
[8] S. Köstlmeier and C. Elsässer, Phys. Rev. B **60**, 14 025 (1999).
[9] G. Möbus and M. Rühle, Ultramicroscopy **56**, 54 (1994).
[10] G. Möbus, R. Schweinfest, T. Gemming, and T. Wagner, J. Microsc. **190**, 109 (1998).
[11] C. Elsässer, N. Takeuchi, K. M. Ho, C. T. Chan, P. Braun, and M. Fähnle, J. Phys. Condens. Matter **2**, 4371 (1990).
[12] B. Meyer Ph.D. thesis, Universität Stuttgart, 1998.
[13] B. Meyer, C. Elsässer, and M. Fähnle, Fortran90 Program for Mixed-Basis Pseudopotential Calculations for Crystals, Max-Planck-Institut für Metallforschung Stuttgart (unpublished).
[14] A. G. Marinopoulos and C. Elsässer, Acta Mater. **48**, 4375 (2000).
[15] Y. Ikuhura, T. Watanabe, T. Saito, H. Yoshida, and T. Sakuma, Mater. Sci. Forum **284–286**, 273 (1999).
[16] C. Elsässer and S. Köstlmeier, Ultramicroscopy **86**, 325 (2001).
[17] H. F. Fischmeister, G. Elssner, B. Gibbesch, K.-H. Kadow, F. Kawa, D. Korn, W. Mader, and M. Turwitt, Rev. Sci. Instrum. **64**, 234 (1993).
[18] J. Bruley, Microsc. Microanal. Microstruct. **4**, 23 (1993).
[19] F. Phillipp, R. Höschen, M. Osaki, G. Möbus, and M. Rühle, Ultramicroscopy **56**, 1 (1994).
[20] P. A. Stadelmann, Ultramicroscopy **21**, 131 (1987).